MRI-Guided Robotic Prostate Biopsy: A Clinical Accuracy Validation

Helen Xu[1], Andras Lasso[1], Siddharth Vikal[1], Peter Guion[2], Axel Krieger[3], Aradhana Kaushal[2], Louis L. Whitcomb[4], and Gabor Fichtinger[1,4]

[1] Queen's University, Kingston, Canada
[2] National Institutes of Health, Bethesda, USA
[3] Sentinelle Medical Inc., Toronto, Canada
[4] Johns Hopkins University, Baltimore, USA
helen@cs.queensu.ca

Abstract. Prostate cancer is a major health threat for men. For over five years, the U.S. National Cancer Institute has performed prostate biopsies with a magnetic resonance imaging (MRI)-guided robotic system. *Purpose*: A retrospective evaluation methodology and analysis of the clinical accuracy of this system is reported. *Methods*: Using the pre and post-needle insertion image volumes, a registration algorithm that contains a two-step rigid registration followed by a deformable refinement was developed to capture prostate dislocation during the procedure. The method was validated by using three-dimensional contour overlays of the segmented prostates and the registrations were accurate up to 2 mm. *Results*: It was found that tissue deformation was less of a factor than organ displacement. Out of the 82 biopsies from 21 patients, the mean target displacement, needle placement error, and clinical biopsy error was 5.9 mm, 2.3 mm, and 4 mm, respectively. *Conclusion*: The results suggest that motion compensation for organ displacement should be used to improve targeting accuracy.

1 Introduction

In the United States, prostate cancer accounts for 25% of cancer incidents in men, making it the second most common cancer among American men. There was an estimated 192,280 new cases and 27,360 deaths in 2009 [1]. The two most common screening methods for prostate cancer are the prostate-specific antigen (PSA) test and the digital rectal exam (DRE). When either test shows abnormal results, needle biopsy is often recommended to determine if a tumor exists and whether it is malignant based on histological analysis.

Each year approximately 1.5 million prostate biopsies are performed and a positive case is found in every 6-8 biopsies. Transrectal ultrasound (TRUS) is currently the standard imaging modality for guiding biopsy due to its low cost and ease-of-use [2]. However, due to the poor image quality of ultrasound, TRUS only has a detection rate of 20-30% [3]. Studies have shown that this method misses the cancer in at least 20% of the cases [4].

Magnetic resonance imaging (MRI) provides an alternative approach to the detection and diagnosis of prostate cancer. It has high spatial resolution, excellent

T. Jiang et al. (Eds.): MICCAI 2010, Part III, LNCS 6363, pp. 383–391, 2010.

soft tissue contrast, and volumetric imaging capabilities [5]. MRI provides clear visualization of the prostate and its substructures including the peripheral zone (PZ), which is the most common location of cancer [6]. It allows suspicious lesions to be identified and guides biopsies at these targeted sites. MRI has not been widely adopted for prostate interventions due to its strong magnetic fields, confined physical space, and high cost.

Krieger *et al.* developed an MRI-guided transrectal robotic prostate biopsy system [7] that has been used in over 200 biopsies to date at the U.S. National Cancer Institute. This paper reports a quantitative longitudinal evaluation of the clinical accuracy of this robotic biopsy system under MRI-guidance. In addition to reporting the difference between the planned and actual biopsy location, this study takes into account organ motion during the procedure, thus quantifying targeting accuracy with respect to the tissue target itself.

A much limited preliminary study was reported previously [8]. In this paper, we present major improvements to the validation framework, which include a three-stage deformable registration of an ensemble of organs and a longitudinal accuracy validation study of a much larger National Cancer Institute data set.

2 Method

2.1 Data Acquisition

During the prostate biopsy procedure, the patient was placed inside the MRI scanner in prone position to acquire a series of 2D high resolution T2 weighted axial volumetric slices of the prostate. From the pre-needle insertion volume, the clinicians selected the biopsy location(s) in RAS (Right, Anterior, Superior) coordinates, where the origin was approximately the center of the prostate. The robot was then used to guide a biopsy needle through the rectum into the target sites within the prostate to collect tissue samples. After the needle was in place, another set of 2D axial volumetric slices was taken to confirm needle placement. We used these pre and post-needle insertion image sets to validate the clinical accuracy of the robotic biopsy system.

2.2 Three-Stage Deformable Target Registration

Developing a target registration algorithm that works well for all patient data sets was a challenging task. The prostate motion upon needle insertion can be extremely complex since it is able to dislocate differently from the surrounding structures. The extent of the movement also varies from patient to patient. In addition, the data was gathered over a period of five years in different clinical trials, under different imaging protocols, by different clinicians. Variations in image resolution, field strength, etc. further increased the difficultly of the task. Our main goal was to find a method that would capture most of the prostate movement for the majority of patients during the biopsy procedure.

The pre and post-needle insertions images were examined and it was found that the main transformation between the two volumes was rigid. Although tissue

deformation may be present, it is expected to provide only minor adjustment to the rigid transformation. Karnik *et al.* have also concluded that the results from rigid and non-rigid registrations were not statistically significantly different ($p > 0.05$) in their transrectal prostate biopsies [9]. This observation is consistent with the conclusions of Misra *et al.* that boundary conditions surrounding the organ dominate the deformation more than the constitutive behavior of the tissue itself [10]. The major body structures around the prostate that are relevant to this study are the rectum and pubic bone.

A two-step 3D to 3D rigid registration was developed to capture prostate motion (Figure 1). Using the Insight Toolkit (ITK), the registration is performed between the pre and post-needle insertion image volumes using mutual information. In the first step of our implementation, the pre and post-insertion volumes are used as the fixed and moving images, respectively. The region of interest consists of the rectum, prostate and pubic bone. This step compensates for prostate motion in coherence with the device and patient. To correct for residual decoupled prostate motion, the resulting image is registered again with the original fixed image using only the prostate as the region of interest. Movement in the superior and inferior direction is penalized because the first step should already have corrected for it. Finally, a B-spline deformable registration using grid size $5 \times 5 \times 5$ on the prostate is performed to serve as fine tuning. This compensates for any possible tissue deformation during needle placement.

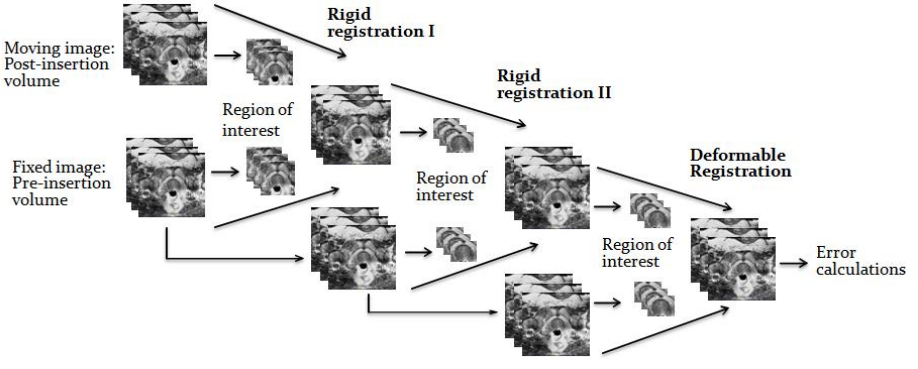

Fig. 1. Three-stage target registration between pre and post-needle insertion images

2.3 Validation of the Three-Stage Registration Scheme

The prostate usually does not show any apparent anatomical feature in the MRI images and it can move practically independently of bony structures. Therefore typical validation methods, such as using landmarks to evaluate the accuracy of the registration are not applicable.

To validate the three-stage registration, we chose to manually segment the prostate, rectum and pubic bone from both the fixed and moving image volumes using ITK-SNAP. Each segmented model was then registered manually

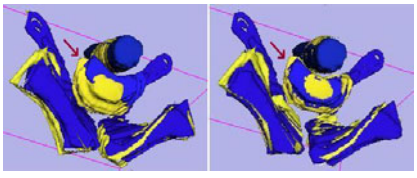

Fig. 2. Contour overlays of the segmented rectum, prostate and pubic bone from moving and fixed images before (left) and after (right) automatic three-stage registration

in 3D-Slicer by aligning the surfaces of the segmented objects in 3D. The results of contour-based prostate registration were compared with the three-stage automatic registration. The bone and rectum indicate the amount of patient movement during the procedure. Figure 2 shows the overlay of a segmented model before and after the automatic three-stage registration.

2.4 Biopsy Accuracy Calculations

Target displacement: The distance between the original and transformed target is calculated as the target displacement (Figure 3). To obtain the transformed target, transformations from the registrations are applied to the original target. To determine whether this movement is related to the needle insertion direction, the displacement is decomposed into two components: one parallel and one orthogonal to the needle vector. A Wilcoxon Signed Rank Test is conducted to see whether prostate movement in the needle direction was significantly larger than the orthogonal one.

Needle placement error: The distance from the original target to the biopsy needle trajectory line is used to represent the needle placement error (Figure 3). This is how much the robot had missed the intended target assuming no prostate motion. The needle trajectory line is obtained by using two needle tip coordinates from the post-insertion volume.

Biopsy error: The distance from the transformed target to the needle trajectory line is defined as the biopsy error (Figure 3). It represents the difference between planned and actual biopsy locations. This measurement is relevant for assessing biopsy accuracy. Since the tissue biopsy core is about 15 mm long, insertion depth is a less important factor.

3 Results

3.1 Registration Accuracy

We selected patients done at 3T that had usable biopsy needle confirmation images and original biopsy target coordinates. A total of 82 biopsies from 21 patients were evaluated. At least one biopsy for each patient was validated using manual contour-based registration method. In addition, all registrations that contained a translation of more than 10 mm were also validated. The prostate contour segmentation error was about 2 mm. When the automatic three-stage

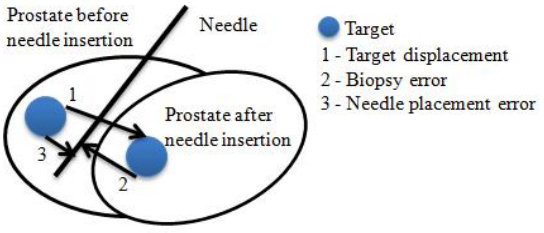

Fig. 3. Diagram illustrating prostate dislocation during needle insertion and biopsy error calculations

registration was off by 3 mm or more, results from the manual registration were used. The registration inaccuracy was mainly due to poor image quality and patient motion. A total of 11 biopsies contained patient movement that was greater than 5 mm. Following contour-based adjustments, all registrations were accurate up to 2 mm. To check the impact of deformable registration on the outcome, it was performed on 20 biopsies from various patients. A Wilcoxon Signed Rank Test was conducted, which showed that the results from deformable registration is not significantly different from the rigid one ($p = 0.54$). This is fully consistent with recent findings of Karnik *et al.* [9].

3.2 Biopsy Accuracy

Table 1 summarizes the mean, range and standard deviation for target displacement, needle placement error, and biopsy error (Figure 3) in all biopsies. To study the impact of patient movement on biopsy accuracy, the results from 11 biopsies which had more than 5 mm patient motion were grouped separately. Figure 4a-c shows the histograms of these three measurements. Lilliefors tests were conducted and it was found that only needle placement errors follow a normal distribution ($p = 0.06$). What follows is that any future needle placement error will have a 95% probability of falling between two standard deviations above or below the mean.

Table 1. The data statistics for biopsy accuracy

	Target Displacement (mm)		Needle Placement Error(mm)	Biopsy Error (mm)	
Mean	5.9	7.2*	2.3	4	4.8*
Range	1-13.4	3.7-11.2*	0.1-6.5	0.5-14.1	1.4-8.8*
Standard Deviation	3.5	2.9*	1.3	2.1	2.3
* Biopsies for patient motion > 5mm only					

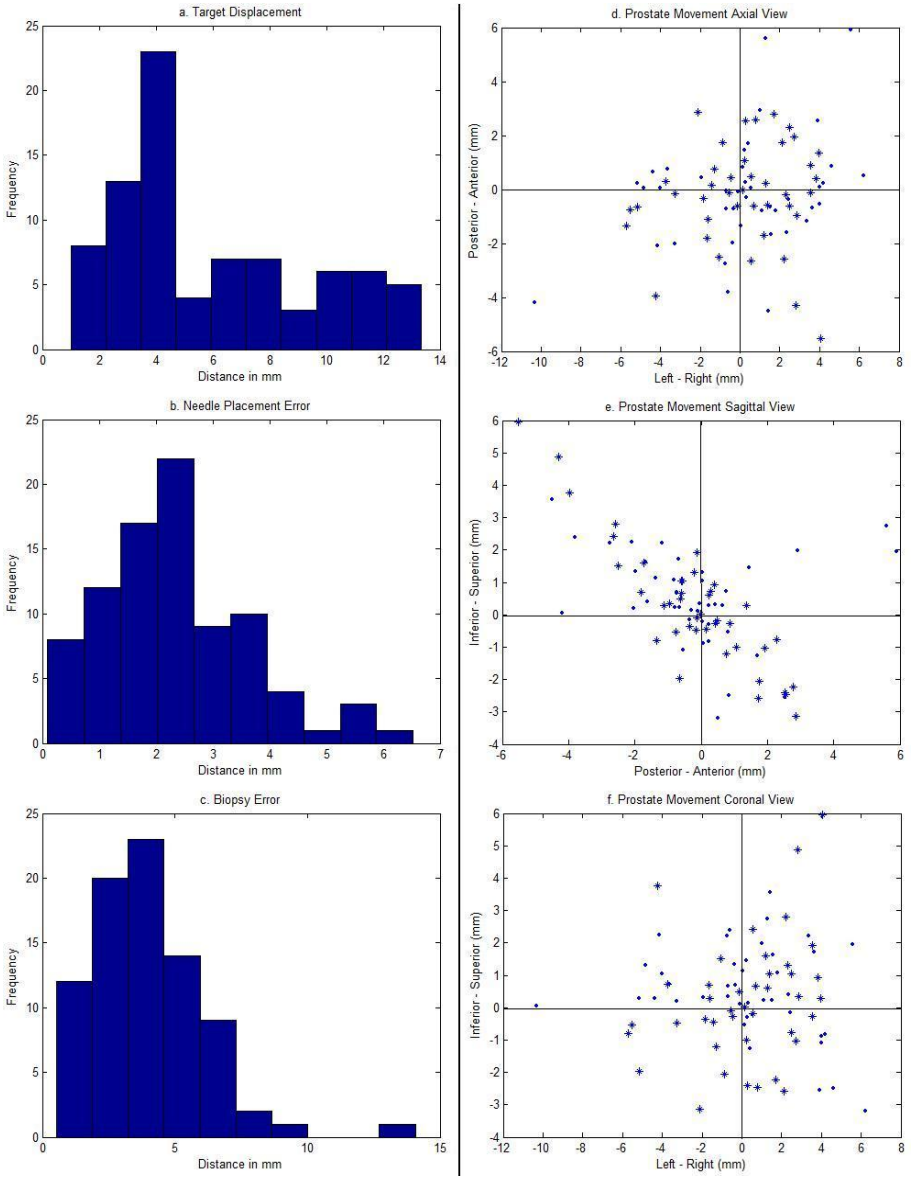

Fig. 4. Left: Histograms of target displacements (top), needle placement errors (middle), and biopsy errors (bottom) of the 82 biopsies. Right: Axial (top), sagittal (middle), and coronal (bottom) view of prostate movement orthogonal to the needle direction. '*' and '.' indicate biopsies taken on the left and right side of the prostate, respectively.

3.3 Target Displacement

Target displacement parallel and orthogonal to the needle direction was also computed. For the parallel component, 46% of the biopsies moved towards the

needle insertion direction (mean: 5.7 mm) and 54% went in the opposite direction (mean: 2.9 mm). The overall average was 4.2 mm in the parallel and 3.4 mm in the orthogonal direction. Results from the signed rank test showed that movement in the parallel direction was not significantly greater than the orthogonal one ($p = 0.36$). For the patient movement larger than 5 mm group, average parallel and orthogonal movement was 3.9 mm and 5.3 mm, respectively.

To analyze the orthogonal displacement component, it was further resolved into movement in RAS coordinates. 73% of the biopsies showed a target movement either towards the superior-posterior (SP) or inferior-anterior (IA) direction (Figure 4e). However, the correlation coefficient between SI and AP was only 0.56. The biopsies were also divided into two categories: left and right side biopsy, with 41 biopsies in each category. 59% of the left biopsies had a positive movement towards right, and 39% of the right biopsies had a positive movement towards left (Figure 4d).

As part of the registration validation process, the segmented rectum and pubic bone were also registered separately. We found that their movements were different from those of the prostate. However, prostate movement was more similar to the bone movement than the rectum movement.

4 Discussion

The mean needle placement error is considered as clinically acceptable since it is less than a clinically significant tumor (2.3 vs. 5 mm). The low error confirmed that the robot is accurate enough in positioning the biopsy needle to hit the intended target. However, this measurement assumes no prostate or patient motion during the procedure. In reality, these two factors usually result in some dislocation of the prostate, causing the target to move. This is evident by the 5.9 mm mean target displacement from the 82 biopsies we studied. The dislocation caused a mean biopsy error of 4 mm, which is on the verge of clinical acceptance.

The 11 biopsies which contained patient movement larger than 5 mm were studied again separately to observe the impact of patient movement on biopsy error. The slight increase in both target displacement and biopsy error suggests that fixating the patient during the procedure may help to decrease biopsy error by only about 1 mm.

The biopsy needle was inserted through the rectum towards the prostate in a mainly superior-anterior direction. It is intuitive to assume that the target should move in a direction along the needle path. Since the statistical test showed that there was no significant difference between target displacement parallel and orthogonal to the needle direction, it means that half of the displacements were in the needle direction. The other half could be due to patient movement during the procedure in addition to the impact of needle insertion.

The separate registrations of the rectum and bone showed that the prostate can move quite independently of these two structures. Since the robotic device was placed inside the patient's rectum, it can limit the rectum's ability to move,

which also explains the observation that prostate movement is more similar to movement of the bone than that of the rectum.

In conclusion, based on validation with segmented prostate contours, our registration algorithm captures the prostate motion during a biopsy with an accuracy of 2 mm. The non-significant impact of deformable registration on the final refinement stage indicates that prostate deformation is less of a factor than organ displacement during the needle placement process. We also found that the pre-planned biopsy target dislocated during the procedure and the prostate motion does differ from both the patient and robot motions. The exact amounts of these motions cannot be known without prostate fiducials or finer volume images. However, even taking into account the imperfection of the segmentation-based validation approach, the results still suggest that further research in organ motion and prostate tracking will be useful to reduce MRI-guided biopsy targeting error. From a sufficient number of biopsy error observations, a statistical model might be built to predict prostate movement during needle placement. Such a model could be used as a reference for clinicians to compensate the insertion plan for predicted movement prior to needle insertion on a prospective patient.

Acknowledgments. We thank C. Menard, A. Singh, J.A. Coleman, R.L. Grubb, J.B. Latouf, and P. Pinto for clinical data collection at the U.S. National Institutes of Health. This work is supported by NIH 5R01CA111288-04 and 5R01EB002963-05.

References

1. Jemal, A., Siegel, R., Ward, E., Hao, Y., Xu, J., Thun, M.: Cancer statistics, 2009. CA Cancer J. Clin. 59(4), 225–249 (2009)
2. Presti Jr., J.: Prostate cancer: Assessment of risk using digital rectal examination, tumor grade, prostate-specific antigen, and systematic biopsy. Radiol. Clin. North Amer. 38(1), 49–58 (2000)
3. Terris, M., Wallen, E., Stamey, T.: Comparison of mid-lobe versus lateral systematic sextant biopsies in detection of prostate cancer. Urol. Int. 59, 239–242 (1997)
4. Wefer, A., Hricak, H., Vigneron, D., Coakley, F., Lu, Y., Wefer, J., Mueller-Lisse, U., Carroll, P., Kurhanewicz, J.: Sextant localization of prostate cancer: comparison of sextant biopsy, magnetic resonance imaging and magnetic resonance spectroscopic imaging with step section histology. J. Urol. 163(2), 400–404 (2000)
5. Susil, R., Ménard, C., Krieger, A., Coleman, J., Camphausen, K., Choyke, P., Fichtinger, G., Whitcomb, L., Coleman, C., Atalar, E.: Transrectal prostate biopsy and fiducial marker placement in a standard 1.5T magnetic resonance imaging scanner. J. Urol. 175(1), 113–120 (2006)
6. Adusumilli, S., Pretourius, E.: Magnetic resonance imaging of prostate cancer. Semin. Urol. Oncol. 20, 192–210 (2002)
7. Krieger, A., Susil, R., Menard, C., Coleman, J., Fichtinger, G., Atalar, E., Whitcomb, L.: Design of novel MRI compatible manipulator for image guided prostate interventions. IEEE Trans. Biomed. Eng. 52(2), 295–304 (2008)

8. Xu, H., Lasso, A., Vikal, S., Guion, P., Krieger, A., Kaushal, A., Whitcomb, L., Fichtinger, G.: Accuracy validation for MRI-guided robotic prostate biopsy. In: SPIE Medical Imaging: Visualization, Image-Guided Procedure, and Modeling, vol. 7625, pp. 762517–762517–8 (2010)
9. Karnik, V., Fenster, A., Bax, J., Cool, D., Gardi, L., Gyacskov, I., Romagnoli, C., Ward, A.: Assessment of registration accuracy in three-dimensional transrectal ultrasound images of prostates. In: SPIE Medical Imaging: Visualization, Image-guided Procedures and Modeling, vol. 7625, pp. 762516–762516–8 (2010)
10. Misra, S., Macura, K., Ramesh, K., Okamura, A.: The importance of organ geometry and boundary constraints for planning of medical interventions. Medical Engineering and Physics 31(2), 195–206 (2009)